Selective inhibitors of the Aurora A-TPX2 protein-protein interaction exhibit *in vivo* efficacy as targeted anti-mitotic agents

Simon R. Stockwell[1,4#], Duncan E. Scott[2,5#*], Gerhard Fischer[3] , Estrella Guarino[1,6], Timothy P. C. Rooney[2,7], Tzu-Shean Feng[2], Tommaso Moschetti[3,8], Rajavel Srinivasan[2,9], Esther Alza[2,10], Alice Asteian[2,11], Claudio Dagostin[2,4], Anna Alcaide[2], Mathieu Rocaboy[3], Beata Blaszczyk[3], Alicia Higueruelo[3,12], Xuelu Wang[3,13], Maxim Rossmann,[3,14] Trevor R. Perrior[15] Tom L. Blundell[3,16], David R. Spring[2], Grahame McKenzie[1,17], Chris Abell[2¶], John Skidmore[2,8*], Marko Hyvönen[3*], Ashok R. Venkitaraman[1,18*]

[1] Medical Research Council Cancer Unit, University of Cambridge, Cambridge CB2 0XZ, UK
[2] Yusuf Hamied Department of Chemistry, University of Cambridge, Cambridge, CB2 1EW, UK
[3] Department of Biochemistry, University of Cambridge, Cambridge CB2 1GA, UK

*Correspondence to:
DES (chemistry), DScott004@dundee.ac.uk
JS (drug discovery), js930@cam.ac.uk
MH (biochemistry), mh256@cam.ac.uk
ARV (biology): arv22@nus.edu.sg

[#] These authors contributed equally

[¶] Deceased

[4] Current address: o2h Discovery, Cambridge, UK

[5] Current address: Drug Discovery Unit, School of Life Sciences, University of Dundee, Dundee, UK

[6] Current address: Spanish National Cancer Research Center (CNIO), Madrid, Spain

[7] Current address: The ALBORADA Drug Discovery Institute, University of Cambridge, Cambridge, UK

[8] Current address: Research & Development, Illumina Cambridge Ltd, Cambridge, UK

[9] Current address: School of Pharmaceutical Science and Technology, Tianjin University, Tianjin, People's Republic of China and Singapore Eye Research Institute, The Academia, Singapore

[10] Current address: Alza & Associates S.L. Sustainable Chemistry, Barcelona, Spain

[11] Current address: Beckman Coulter, Marseille, France

[12] Current address: Exscientia, Oxford, UK

[13] Current address: AstraZeneca, Cambridge, UK

[14] Current address: Cambridge Institute for Medical Research, University of Cambridge, Cambridge, UK

[15] Excellium Consulting, Bury St Edmunds,UK

[16] Current address: Heart and Lung Research Institute, University of Cambridge, Cambridge, UK

[17] Current address: Mosaic Therapeutics, Cambridge, UK

[18] Current address: Cancer Science Institute of Singapore, National University of Singapore, Centre for Translational Medicine, Singapore; Institute of Molecular & Cell Biology (IMCB), Agency for Science, Technology & Research (A*STAR), Singapore

Abstract

The protein kinase Aurora A, and its close relative, Aurora B, regulate human cell division. Aurora A is frequently overexpressed in cancers of the breast, ovary, pancreas and blood, provoking genome instability and resistance to anti-mitotic chemotherapy. Intracellular localization and enzymatic activity of Aurora A are regulated by its interaction with the spindle assembly factor TPX2. Here, we have used fragment-based, structure-guided lead discovery to develop small-molecule inhibitors of the Aurora A-TPX2 protein-protein interaction (PPI). These compounds act by novel mechanism compared to existing Aurora A inhibitors and they are highly specific to Aurora A over Aurora B. We identify a biophysically, structurally and phenotypically validated lead compound, **CAM2602**, exhibits oral bioavailability, favourable pharmacokinetics, pharmacodynamic biomarker modulation, and arrest of growth in tumour xenografts. Consistent with our original finding that Aurora A overexpression drives taxane-resistance in cancer cells, **CAM2602** synergizes with paclitaxel to suppress the outgrowth of pancreatic cancer cells. Our results provide a structural and chemical blueprint for targeting the Aurora A-TPX2 PPI for cancer therapy and suggest a promising clinical utility for this mode of action.

Key words: Aurora A, TPX2, fragment-based drug discovery, cancer, protein-protein interaction

Introduction

Aurora A is a serine/threonine protein kinase that plays an important role in controlling early stages of mitosis, including centrosome maturation and separation, mitotic entry, and bipolar spindle formation[1,2]. Aurora A may be upregulated in cancer cells as a consequence of chromosome rearrangements, aberrant gene expression, or through protein stabilisation. Aurora A overexpression is a common feature of several cancers including ovarian, prostate, pancreas and breast, and has been linked to poor treatment outcome[3-5]. Disruption of the spindle assembly checkpoint due to Aurora A overexpression promotes tumourigenesis via chromosomal instability and aneuploidy[3,5,9,10]. Conversely, genomically-unstable cancer cells may become critically reliant on Aurora A function[11,12]. Androgen-receptor positive models of castration-resistant prostate cancer also show significant sensitivity to Aurora A inhibition[13]. Furthermore, non-genetic elevation of Aurora A levels is reported to drive resistance to current generation EGFR inhibitors in non-small cell lung cancer models[14] and tumour resistance to taxanes is a further consequence of aberrant expression[15,16]. Aurora A inhibitors are also increasingly finding use against AML and related leukaemias[6-8]. Consequently, the cancer therapeutic promise of an effective inhibitor of Aurora A is of much interest and the focus of multiple drug discovery studies[17-19].

Targeting protein for *Xenopus* kinesin-like protein 2 (TPX2) is a spindle assembly factor essential for mitotic spindle organisation, maintaining spindle-pole integrity and microtubule nucleation[20]. Its interaction with Aurora A mediates localisation of Aurora A to spindle microtubules[21], regulates Aurora A kinase activity by stabilization of the active protein[22,23] and protects the activating Thr288 residue in the catalytic domain of Aurora A from the action of PP1 phosphatase[24,25]. Aurora A and TPX2 are frequently co-overexpressed in tumours[26], therefore the association of Aurora A and TPX2 comprises a novel oncogenic unit that presents a promising target for cancer therapy[1,22].

Significant effort has been applied to developing ATP-competitive inhibitors of the Aurora kinases and several have progressed to clinical trials[17,27,28]. Reported Aurora A inhibitors bind to the highly conserved ATP-binding site of the kinase and consequently exhibit variable selectivity for Aurora A

over related kinases, most notably Aurora B and Aurora C[17,29]. High similarity between Aurora A and Aurora B , especially in their catalytic sites[30], makes it challenging to develop highly selective small molecule inhibitors for Aurora A. Alisertib (MLN8237)[31], an Aurora A inhibitor in clinical trials, is reported to have a selectivity for Aurora A over Aurora B of approximately 200-fold[32], although work using cellular assays to profile and characterise Aurora A inhibitors has indicated an order of magnitude lower specificity[18,31]. A modest number of early studies have pursued orthogonal approaches to Aurora A inhibition not dependent directly on competition with ATP. These approaches include ATP-competitive inhibitors that allosterically disrupt the Aurora A interaction with N-Myc or through direct orthosteric competition at the site of a PPI with functional binding partner proteins, such as TPX2[33-37]. It is established that kinase inhibitors that target sites other than the ATP-pocket can lead to improved selectivity and novel pharmacology[38,39]. Additionally, therapeutically targeted PPIs are less likely to accommodate mutations without loss of protein function, therefore reducing the potential for emergence of resistance[40,41].

Although ATP-binding site inhibitors that allosterically disrupt the interaction of Aurora A and N-MYC have demonstrated efficacy in xenografts[42], to date, no reported PPI inhibitors of Aurora A-TPX2 have exhibited the potency or pharmacokinetics to be advanced to *in vivo* pre-clinical models. By targeting the TPX2 binding site unique to Aurora A, we aim to develop a small molecule inhibitor of Aurora A which is expected to show the therapeutic potential demonstrated by clinical agents such as alisertib and which additionally avoids the selectivity issues that typify ATP-competitive molecules. Moreover, by disrupting binding to a scaffolding protein TPX2, we hope to achieve also greater efficacy or new biological effects through the different mechanism of action.

Results

Development of CAM2602

Fragment-based drug design

We have pursued a structure-guided fragment-based drug development approach. Briefly, a library of 600 fragments was screened by thermal shift in the presence of an ATP-site binding inhibitor. Thermal shift hits were progressed into a ligand-based NMR experiment, and a number of these such as 3-hydroxybenzoic acid (**1**) were shown to bind Aurora A and could be displaced by a TPX2 peptide fragment (amino acids 7-22) but not by a tight-binding ATP-site ligand. However, these NMR hits had no measurable activity in a fluorescence polarisation (FP) assay measuring inhibition of Aurora A's interaction with labelled TPX2. Moreover, electron density could not be observed in X-ray crystallographic soaks. A focussed iteration of chemical elaboration of these hits yielded further fragments that maintained the desired competition profile in ligand-based NMR experiments, possessed activity in the FP assay, showing K_D values of around 1 mM (pK_D ~3) and were confirmed to bind to Aurora A by isothermal titration calorimetry (ITC). Crucially, we were also able to obtain crystal structures of some of these hits in complex with the Aurora A protein, enabling structure-based drug design. A representative such fragment is compound **2**, a biphenyl molecule bearing a carboxylic acid and phenol group on one ring and a lipophilic trifluoromethoxy on the other. Compound **2** has a K_D 63 µM as measured by our competitive FP assay and K_D of 145 µM as determined by ITC. The binding of **2** to Aurora A, as determined by X-ray crystallography, alongside some key structural motifs showing both the ATP site and TPX2 peptide binding sites, is highlighted in **Fig. 1A**. Our NMR and FP studies showed that these fragments are competitive with the TPX2 peptide (**Supplemental Fig. S1**) and X-ray crystallography revealed that the hit fragments bind to part of the TPX2 binding site (**Fig. 1B** and **1C**), otherwise occupied by the Tyr8 and Tyr10 of TPX2 (we will refer to this pocket as the "tyrosine pocket" in the subsequent discussions) (**Fig. 1C**).
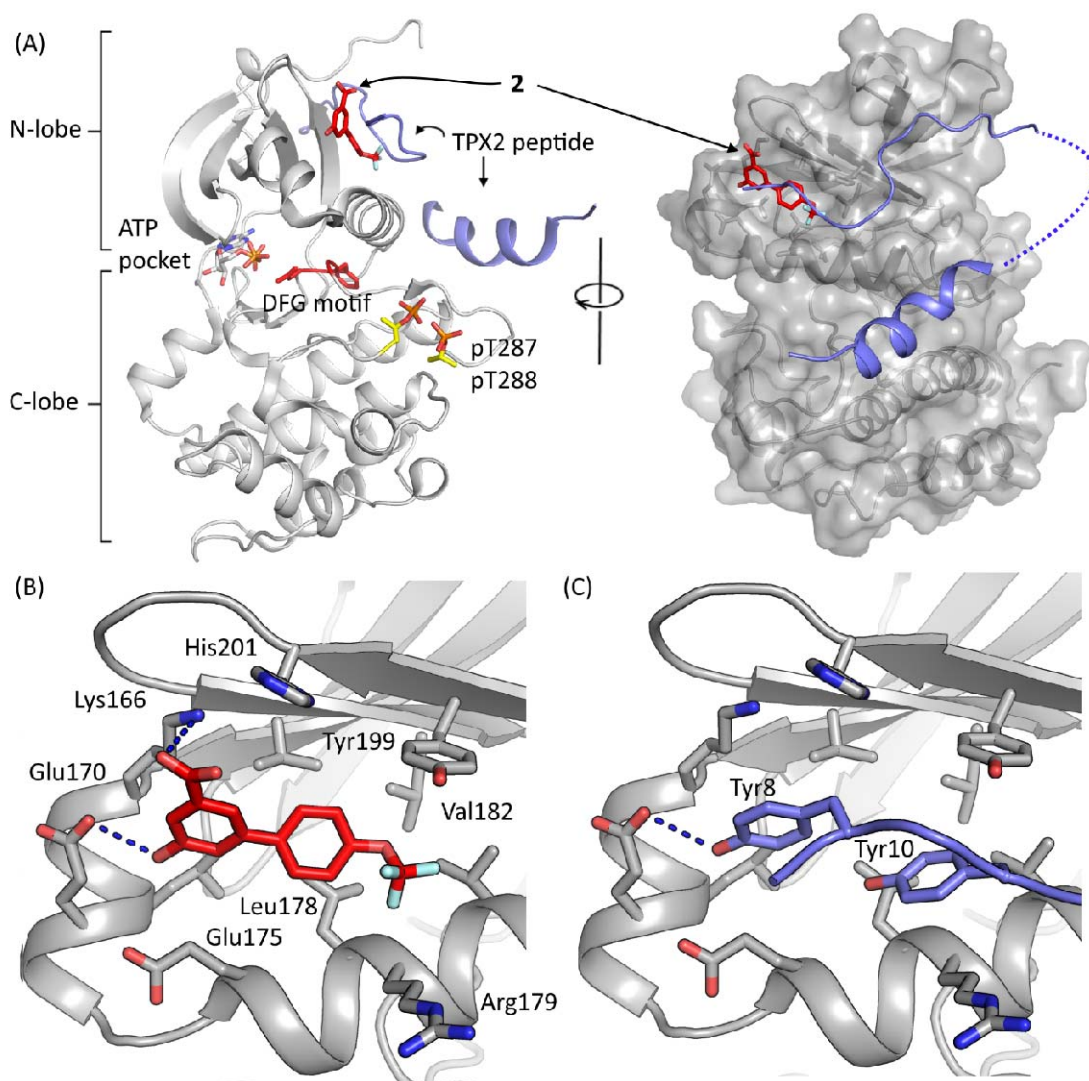
Figure 1. Hit molecule engagement with Aurora A "tyrosine pocket". (A) Superposition of developed hit fragment **2** (red sticks, PDB code: 8C1M) onto Aurora A kinase bound to TPX2 peptide, showing key kinase regulation moieties (PDB: 1OL5). The TPX2 peptide is superimposed for reference as blue cartoon (from PDB code: 1OL5), the phosphorylated threonine residues Thr287 and Thr288 are shown in yellow on the activation loop. The DFG motif (red sticks) and ATP are also shown for reference. **(B) 2** (red carbons) bound to the surface of Aurora A. Key interactions with Lys166 and Glu170 are shown. **(C)** For comparison, TPX2 (blue carbons and chain, PDB:1OL5) overlayed with Aurora A from complex with **2**. In particular, the interaction of Tyr8 from TPX2 with Glu170 of Aurora A is highlighted.

Through a further iterative development of the inhibitors utilising X-ray structure-based drug design and biophysics (FP and ITC), we improved the affinity of our weak, millimolar fragments hits by over 10,000-fold to generate the lead compound **CAM2602** with a K_D of 20 nM for Aurora A and a ligand efficiency of 0.33 (**Fig. 2A** and **S1** and **S2**). An early modification was to change the phenol group of **2** into indole whilst replacing the trifluoromethoxy with a smaller chlorine to give **3**, which improved the K_D to 1.26 μM (**Fig. 2D**). The indole-aryl core of the molecule lays in a hydrophobic pocket assembled from Leu169, Leu178, Val182, Val206 and the side chain of Lys166. The indole nitrogen proton seems to form a hydrogen bond with the side chain of Glu170 thus mimicking the phenol of

Tyr8. The carboxylic acid group was observed to bind to interact with Lys166 and His201. Further, the electron density supported it being twisted from the plane of the indole ring in order to form a salt-bridge with Aurora A (**Fig. 1B**). Our analysis of ligands in PDB and CSD[43] databases show that carboxylic acids are more commonly in-plane with the aromatic ring (data not shown) and presumably this twisting incurs an energetic penalty upon binding. To minimise the loss of binding energy and to stabilise the torsional twist in the ground state, we introduced an *ortho* methyl group to **4** (K_D 630 nM). We found that introduction of a *meta* nitrile group in the *para*-chloro ring led to a further modest improvement in potency and the crystal structure of Aurora A in complex with **5** revealed that the induced movement of Tyr199 generated a small pocket between Tyr199 and His201 (the "*meta*-channel"). **5** had reasonable FP activity and good cell permeability meaning that it could be used as a tool, particularly for early cell-based experiments. However, its potential utility *in vivo* is primarily hampered by poor hepatocyte stability, which was improved significantly through the introduction of isosteric replacements for the carboxylic acid, particularly acyl sulfonamides, in compounds **6** and **7**. In addition it was found that the *meta*-channel between Tyr199 and His201 could be further exploited by the replacement of the nitrile with an heteroaryl ether, to give **8** and lead compound **CAM2602** which the new heterocycle T-stacks with Tyr199.

Our lead series compounds are a biophysically and structurally validated set of 4-phenylindoles that bind in the TPX2 binding pocket on the surface of Aurora A and can inhibit the binding of TPX2 peptide to Aurora A. Our lead series maintains the acidic group present in fragment **2**, either as a carboxylic acid or an acylsulfonamide, whilst the phenol has been replaced with an NH in the form of an indole. Data for a small selection of key compounds is exemplified in **Fig. 2B**. An overlay of the crystal structures of the early hit **2** with **CAM2602** bound to Aurora A reveals a remarkable overlap of the core biaryl scaffold in the two compounds (**Fig. 2C**).
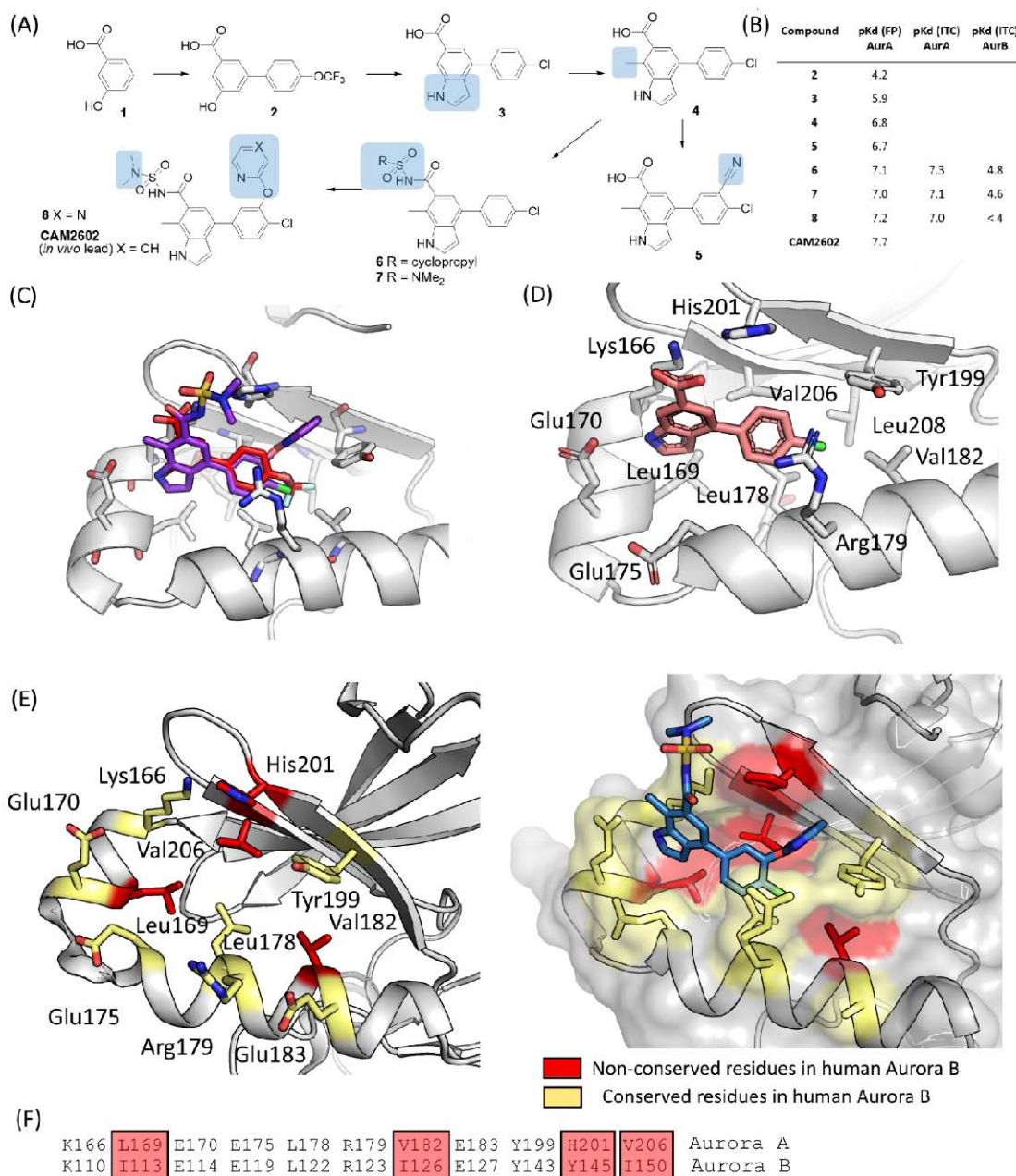
Figure 2. Representative lead molecules and the basis of selectivity against Aurora B (A) Overview of the fragment-based development of **CAM2602** to inhibit the Aurora A:TPX2 protein-protein interaction. The blue boxes highlight the key change(s) at each step. **(B)** Biophysical FP and ITC pK_D values against Aurora A and Aurora B are shown for the compounds. **(C)** The X-ray crystal structure of fragment **3** bound to Aurora A is shown (red carbons; PDB: 8C1M) overlaid with the lead **CAM2602** (purple carbons; PDB: 8C1K). **(D)** Complex of **3** (pink carbons; PDB: 8C15) with Aurora A with residues in the Tyr pocket highlighted. **(E)** Conservation of residues in the Tyr pocket between Aurora A and B with identical residues coloured in pale yellow and non-conserved residues coloured red, shown on Aurora A without a ligand (PDB: 1OL5) and on Aurora A in complex with **7** (PDB: 8C1G).. **(F)** Sequence alignment of human Aurora A and B with differences in residues indicated. Residues in red boxes are non-conserved.

Kinase selectivity

Given our inhibitors bound to a PPI site, we hypothesised that they would show high selectivity for Aurora A over other kinases including Aurora B. Achieving selectivity over Aurora B has been recognized as a desirable feature of new drugs, but thus far challenging to achieve, due to the high sequence similarity (>70% identity) between the two kinase domains[2,24,44,45] and the presence of a site that is analogous, to the TPX2 binding site that, in the case of Aurora B, binds to the protein INCENP. Although many key residues that interact with their respective ligands are conserved, the shape of the base of the pocket is altered by three changes. In particular, His201, which in Aurora A is an important sidechain that forms a π-stack with the heterocyclic ethers and potentially participates in a charged interaction with the sulfonamide moiety in our lead compounds, is a tyrosine residue in Aurora B (Tyr145). Val182 and Val206 of Aurora A are both replaced by isoleucines in Aurora B, with the extra methyl groups making the Aurora B pocket somewhat smaller (**Fig. 2E, F**).

We evaluated the selectivity of our Aurora A:TPX2 inhibitors thoroughly; we measured binding of a small panel of compounds to Aurora A and B by direct binding assays and we also determined wider selectivity through assessment of competitive binding against an ATP-site ligand for a panel of representative kinases. Firstly, using ITC, the binding of lead series representatives **6**, **7** and **8** was measured to both Aurora A and Aurora B. As expected, a good correlation is observed between the K_D our inhibitors for Aurora A as derived from competitive FP experiments and that from direct binding to Aurora A by ITC. Additionally, we observe an approximate 300-fold selectivity for Aurora A over Aurora B for **6** and **7**. With the introduction of a meta-ether substituent in **8**, the compound's potency against Aurora B was too weak to be measured – indicating greater than 1000-fold selectivity for Aurora A (**Fig. S2**). The specificity of **8** for Aurora A over Aurora B is at least as great as the best compounds reported previously [18,46]. As a further validation of the target specificity of our PPI inhibitor approach, **8** showed little ATP-site competition at 10 µM in a screen against 97 different kinases (**Fig. S3**).

Toxicity

To evaluate the toxicity of our molecules we examined **6** and the lead compound **CAM2602** in protein based Cerep panels, cellular toxicity assays, and peripheral blood mononuclear cells (PBMC) assays. High content cell toxicology of **6**, up to 40 µM in HepG2 cells, indicates that there were no measurable effects on cell growth, nuclear size, DNA structure, cell membrane permeability, mitochondrial mass, mitochondrial membrane potential or cytochrome c release (**Table S1**). Compound **6** shows no off-target activities in Cerep ExpresSProfile screen (55 GPCRs, transporters and ion channels), at 10 µM (**Table S2**). Lead compound **CAM2602** exhibits only one off-target activity in this screen inhibiting binding of an agonist radioligand to human adenosine 3 (A3) GPCR by 55% at 10 µM. **CAM2062** does not inhibit hERG, or a panel of CypP450 enzymes at 25 µM. Some of the ADMET properties of **CAM2602** are shown in **Table S3**.

Mechanistic characterisation of the Aurora A:TPX2 inhibitors
Target engagement in cells induces Aurora A mislocalisation

Previous reports have shown that Aurora A is recruited to the mitotic spindle through its protein-protein interaction with TPX2 [21,22]. We have previously reported a high-content screening assay in which we can detect as the displacement of Aurora A from the spindle in mitotic cells[37]. Here we used this assay to provide a measure of cellular target-engagement for our key compounds (**Fig. 3**). In parallel, we performed a related high-content assay measuring loss of the activating

phosphorylation at threonine 288 (P-Thr288) on Aurora A. In agreement with previous data[37], the EC_{50} values in these two assays were well-correlated (**Fig. 3A, B**).
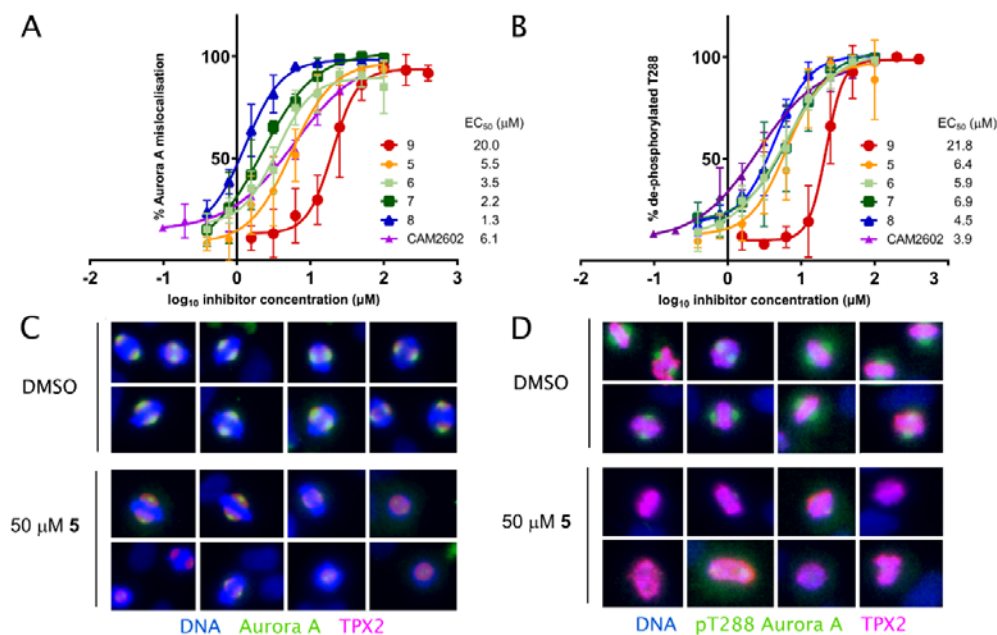

Figure 3. High content microscopy assays show mislocalisation of Aurora A from the mitotic spindle or loss of phospho-Thr288 Aurora A in mitotic nuclei when treated with inhibitor. **(A)** HeLa cells were treated with titrations of the indicated compounds for 2 hours before being fixed, stained for Aurora A and analysed using high-content microscopy to determine the percentage of observed mitotic cells at each concentration with spindle-displaced Aurora A (mislocalisation). The indicated EC_{50} values for each compound were calculated from the plots of assay scores against compound concentration. **(B)** As in A but stained for dephosphorylated Thr288 Aurora A. **(C)** Representative images of mitotic cells imaged in the mislocalisation assays treated either with DMSO vehicle or with 50 μM **5** and stained for DNA (blue), Aurora A (green) and TPX2 (purple). **(D)** As in C, but stained for phosphorylated Aurora A instead of total Aurora A.

Impact on viability in dividing cancer cells

Blocking the protein-protein interaction between Aurora A and TPX2 is predicted to disrupt Aurora A function in dividing cells[20] leading to defects in spindle assembly, transient activation of the spindle assembly checkpoint and eventual apoptosis in a post-mitotic G1 arrest[47]. Actively cycling cells experiencing Aurora A inhibition are, therefore, expected to exhibit eventual loss of viability due to prolonged disruption of Aurora A function. The compounds were titrated in the growth assay to estimate their cytotoxic impact against either Jurkat acute T cell leukaemia cells or HeLa cervical adenocarcinoma. In general, we observed lower GI_{50}s in compound treatments with Jurkat cells (**Fig. S4**). To explore the potential therapeutic window for our compounds in dividing cancer cells versus normal tissues we made use of peripheral blood mononuclear cells (PBMCs). PBMCs are viable in tissue culture conditions, but do not cycle in the absence of a lymphocytic stimulus such as anti-CD3/CD28[48,49]. Non-cycling cells should not require active Aurora A, so assessing cell viability in the PBMCs may serve an indirect measure of potential off-target toxicity. We observed that most of the compounds with cell activity in HeLa and Jurkat cell viability experiments had no impact on the non-cycling PBMC cells when applied at less than 200 μM, which was an order of magnitude greater than the typical GI_{50} values seen in the equivalent Jurkat cell data (**Fig. S5**). As a control, the PBMC cells

were also treated with ATP-competitive Aurora A inhibitor, alisertib, which also demonstrated no toxicity in the PBMC cells. Treatment of PBMCs with staurosporin, a non-selective kinase inhibitor that exhibits promiscuous cytotoxicity, yielded dose-related cell killing, indicating that the assay was
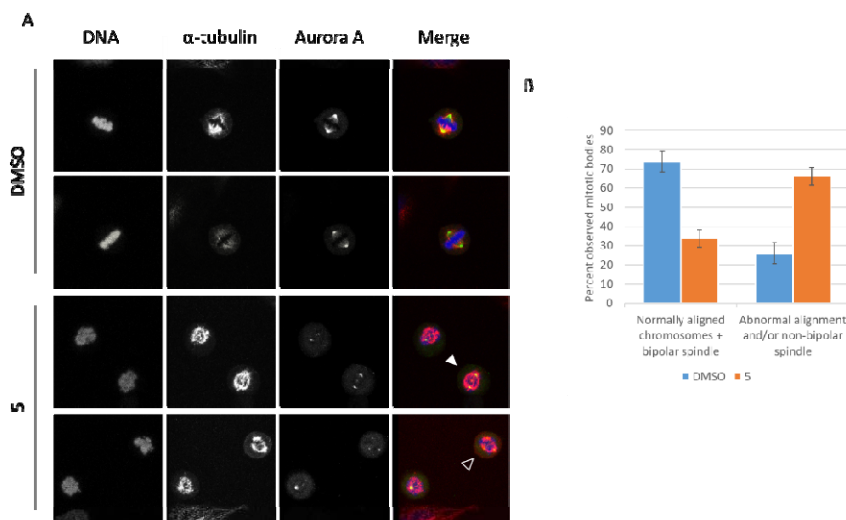
capable of reporting non-specific cell-killing effects.

Figure 4. Mitotic spindle abnormalities in cells treated with 5 (A) HeLa cells were treated with 50 μM (1x GI$_{50}$) **5** or DMSO for 6 hours prior to being fixed, fluorescently stained for the indicated proteins or DNA and imaged using confocal microscopy. Two representative fields containing mitotic cells are shown for both treatment conditions. Mitotic cells were enumerated to exhibit spindle abnormalities if they demonstrated unaligned chromosomes and/or non-bipolarity, examples of which are indicated by the solid and outline arrowhead, respectively. **(B)** Relative proportions of normal and abnormal spindle classes across all imaged mitotic cells for both DMSO and **5** treated cells (>100 mitotic cell observations). Error bars show standard deviations from the mean (n=3 image sets per condition).

Disruption of the Aurora-A:TPX2 interaction results in spindle abnormalities

An acute cellular consequence of inhibiting the mitotic function of Aurora A is the appearance of spindle abnormalities in those cells undergoing mitotic division[50,51]. Driven by deregulation of centrosome maturation and spindle pole forces, the abnormalities can be broadly characterised as including loss of spindle bipolarity and/or misalignment of the condensed chromosomes at the metaphase spindle; observations of these phenotypes have been used in pre-clinical and clinical studies employing ATP-competitive Aurora A inhibitors[32,52,53]. Here, we treated HeLa cells with either a DMSO vehicle control or **5** for 6 hours before preparing them for microscopy using fluorescent labels for chromatin DNA, Aurora A and α-tubulin proteins. Pro-metaphase, metaphase and anaphase mitotic cells from each treatment condition were readily identified over non-mitotic cells by the characteristic condensed chromosomes and the presence of α-tubulin-containing spindles. Frequent examples of mitotic cells with misaligned or trailing chromosomes in addition to examples of monopolar spindles and spindles with more than two poles were seen following 6 hours of compound treatment (**Fig. 4A, 4B**). Importantly, immunostaining of the mitotic cells reveals association of Aurora A with mitotic spindles in vehicle-only control cells, while treatment with **5** produced a clear displacement of Aurora A from these structures. Overall, target engagement in the

acutely treated cells led to Aurora A displacement and the spindle abnormality phenotypes expected from prior studies on the phenotypes arising from the inhibition of Aurora A activity, and/or its PPI with TPX2.

PPI inhibitors of Aurora A-TPX2 demonstrate synergy with taxanes

Aurora A overexpression drives resistance to taxanes in cancer cells[15,16,54]. In addition, compelling data indicates that inhibition of Aurora A synergises with paclitaxel in cell lines exhibiting Aurora A amplification[55]. Using an early lead compound, **5**, we explored whether our Aurora A-TPX2 inhibitors would also exhibit synergy with taxanes when applied to cancer cells. We employed a previously reported experimental protocol for synergy calculation[55], in which the PANC-1 pancreatic ductal adenocarcinoma cell line was treated for 72 hours with a matrix of Taxol and Aurora A inhibitor concentrations, followed by assessment using a viability assay to estimate impact on cell survival from each compound combination (**Fig. 5A,B**). It was apparent that low doses of these single agents, insufficient by themselves to induce any cytotoxicity, greatly reduced cell viability when used in combination; dosing the PANC-1 cells with 1.88 nM Taxol or 25 µM **5** alone resulted in a 6% or 3% fall in cell viability at 72 hours post-treatment, respectively, whereas combination of 1.88 nM Taxol with 14 µM **5** gave a 50% drop in viability. This combination effectively reduced the GI_{50} of **5** in PANC-1 cells by 3.8-fold from 54 µM (**Fig. 5C**). We estimated synergy by comparison of observed dose response outcomes across the matrix with predicted outcomes assuming additivity according to the Bliss model (**Fig. 5D**).[55,56] This approach indicated that the most significant drug synergy was detected using a concentration of 25 µM compound **5** and 1.88 nM Taxol. Comparison of the final survival scores for these concentrations applied singly to PANC-1 cell for 72 hours versus the corresponding Bliss model-predicted and observed scores for combination of the two showed a dramatic impact upon treatment with Taxol and **5** in combination (**Fig. 5E**).
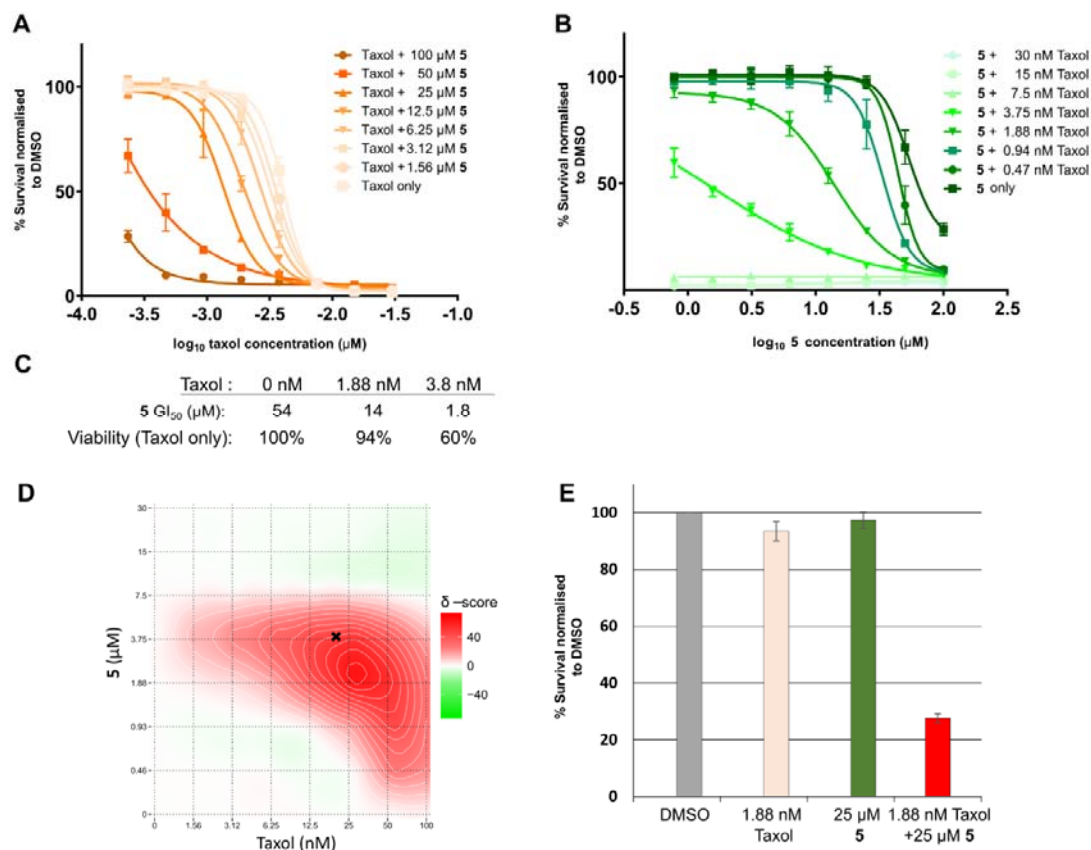
Figure 5. **Aurora A:TPX2 PPI inhibitors synergise with Taxol in PANC-1 cells. (A)** and **(B)**: PANC-1 cells were dosed with a matrix of concentrations of Taxol and **5**, including single agent and vehicle controls for all concentrations tested. 72 hours following treatment, the cells were assayed for remaining viability relative to vehicle controls. **(C)** Table showing effective decrease in **5** GI_{50} in PANC-1 cells when combined with increasing concentrations of Taxol. Also shown are the corresponding viability changes effected by Taxol if applied as a single agent. **(D)** The vehicle-normalised viability assay data were processed using SynergyFinder webserver (https://synergyfinder.org/)[57], producing a heatmap indicating the presence of synergy (red) or antagonism (green) between the two drugging agents when compared to modelled predictions of additivity **(E)** Chart comparing vehicle-normalised 72-hour viability assay values between single agent and combined treatments of the concentrations of Taxol and **5** yielding the greatest synergic effect. The single-agent inhibition values for Taxol alone or **5** alone were used to calculate a drug combination surface under the assumption of an additive effect using SynergyFinder, which is shown as the 'predicted' value. Bars show standard deviations from the mean (n=4).

Biomarkers of Aurora A-TPX2 disruption

Phosphorylation of serine 10 on histone H3 (PH3) has been used as an indicator of mechanistic target engagement for ATP-competitive Aurora A inhibitor alisertib[32,58-60]. Aurora A inhibition produces a delayed G2/M transition driving accumulation of PH3 through the activity of Aurora B[61,62]. We treated Jurkat cells with either an early lead compound (**6**), alisertib or a vehicle control and followed PH3 levels over time by western blotting. Accumulation of PH3 in Jurkat lysates was observed from 16 hours following treatment both with alisertib and **6** (**Fig. 6A**).

It has previously been shown that PH3 accumulation in tumour cells treated with Aurora A inhibitors is detectable from as early as 4-6 hours with microscopy [32,59]. This suggests a sensitivity advantage for techniques that can resolve mitotic cells in asynchronous cell samples, so we next explored flow cytometry for detection of PH3 and phospho-Thr288 changes in Jurkat cells treated *in vitro* with varying GI_{50}-multiples of **6** or a vehicle control for 8 hours. Supporting validation of PH3 immunostaining in these samples, this marker was only detectable in mitotic cells, identifiable by their 4n DNA (**Supplementary Fig. 6**). Samples treated with **6** demonstrated a consistent increase in PH3-positive mitotic cells compared to vehicle controls (**Fig. 6A, B**). A 2x GI_{50} dose of **6** yielded almost a 3-fold increase in mitotic cells compared to DMSO exposure, with a similar magnitude of increase at a 5x GI_{50} dose. Complementing the PH3 data, decreased P-Thr288 Aurora A was observed in the mitotic cells treated with **6**. This detection of biomarker modulation was repeated for the lead compound, **CAM2602,** with alisertib as a positive control (**Fig. 6C**). Under these conditions, both **CAM2602** and alisertib treatment exhibited similar evidence of Aurora A inhibition.
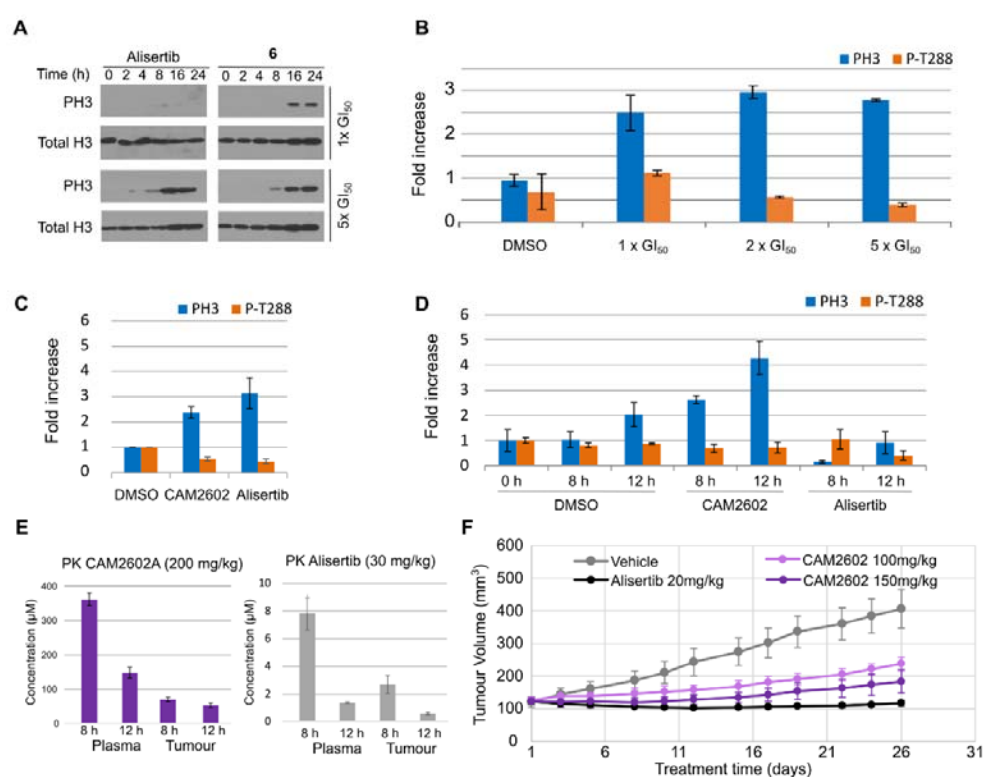
Figure 6. *In vitro* and *in vivo* characterisation of CAM2602 and analogues. **(A)** Western blot analysis of PH3 levels in Jurkat cells treated with the indicated fold-GI_{50} equivalents of alisertib (7 or 35 nM) and **6** (20 or 100 µM). **(B)** Flow cytometric analysis of Jurkat cells treated with a range of fold-GI_{50} concentrations of **6** (1x GI_{50} = 20 µM) for 8 h. The cells were stained for DNA, PH3 and P-Thr288 Aurora A and were analysed to determine the proportion of mitotic cells (having both 4n DNA and PH3 positivity); additionally, the proportion of cells positive for P-Thr288 within the mitotic population was also measured per treatment condition. Data is plotted as normalised values relative to the untreated control. (See **Fig. S6** for the flow cytometry data and for the gating strategy.) **(C)** Jurkat cells were treated for 8 hours with 20 µM **CAM2602** or 14 nM alisertib and analysed by flow cytometry for PH3 positive cells relative to vehicle controls. PH3-positive cells from each sample were assessed for loss of P-Thr288 positivity. **(D)** Female NOD scid gamma (NSG) mice bearing solid Jurkat tumours (subcutaneous implantation, rear dorsum) were administered a single oral dose of

either **CAM2602** or vehicle. Tumour cells from 0, 8 or 12 hours of treatment were analysed by flow cytometry similarly to *in vitro* samples in panel B **(E)** Pharmacokinetic analysis of CAM2602 or alisertib concentrations in tumour and plasma samples taken at 8 or 12 hours following dosing with 200 mg/kg and 30mg/kg, respectively. (F) NSG mice bearing subcutaneous, solid tumour xenografts of Jurkat cells were dosed orally once per day with either vehicle, **CAM2602** or alisertib, as indicated (n=5). Tumour volumes were estimated periodically over the 26 days of dosing by calliper measurement. Error bars show standard deviations from the mean.

PPI inhibitor of Aurora A-TPX2 demonstrates *in vivo* activity

Given the favourable ADMET profile of **CAM2602** (**Table S3**) and its ability to modulate biomarkers of target engagement *in vitro*, we next sought to demonstrate that **CAM2602** could affect tumour cell biomarker modulation *in vivo* following acute systemic administration in a mouse xenograft model.

We assessed first the pharmacokinetics of **CAM2602** by administering the compound at 3 separate doses in female CD-1 mice and measuring the total concentration of compound in plasma over time (**Fig. S7)**. The intravenous dose is cleared in a first-order elimination process. At higher doses, administered orally, the concentration of compounds rapidly reaches a plateau that is maintained for at least 8 hours. These clearance profiles suggest that one or more clearance mechanisms, i.e. efflux and/or metabolism may be saturated at these compound doses. The oral bioavailability of **CAM2602** at 50 mg/kg was 99.8% while no weight loss or adverse events were observed in any PK studies.

For the xenograft model, Jurkat cells were engrafted as a subcutaneous, solid tumour in the flanks of NOD SCID gamma (NSG) mice. Xenografted mice were orally administered a single dose of 200 mg/kg **CAM2602**, 30 mg/kg alisertib or vehicle. Doses were chosen based on our earlier PK data for **CAM2602** (**Fig. S7**) or from equivalent, previously reported studies using alisertib[32,63,64]. Tumour and plasma samples were then taken 8- or 12-hours post-dosing. Resected tumours were digested into single cell aspirates, fixed and processed using flow cytometry to detect modulation of PH3 and P-Thr288 biomarkers (**Fig. 6D**). At both 8- and 12-hours post-dosing, xenografted tumour cells from **CAM2602**-treated mice demonstrated fold-increases in PH3 over vehicle controls matching those seen previously *in vitro* (**Fig. 6B, 6C**). Across the **CAM2602**-treated tumour samples, decreases in the Aurora A P-Thr288 marker were also evident, but changes to this marker were considerably less pronounced than those seen for *in vitro* conditions and were not significant. Plasma and tumour concentrations of **CAM2602** exhibited high micromolar concentrations of the compound in both compartments at both 8- and 12-hour time points (**Fig. 6E**). When adjusted for mouse plasma protein binding (**table S3**) the predicted free drug concentrations in plasma (5.4 µM at 8 hours and 2.2 µM at 12 hours) are well in excess of the K_D (20 nM) for the target, supportive of likely target engagement. Moreover, the measured tumour concentrations (70 µM at 8 hours and 54 µM at 12 hours) suggest meaningful tissue exposure consistent with levels required for inhibition in cells up to 12-hours post-dosing. Contrary to our *in vitro* data (**Fig. 6A, 6C**), tumour samples recovered from alisertib-treated mice yielded a decrease in PH3 at 8 hours, and neither 8- or 12-hour samples yielded the increase in PH3 expected from Aurora A inhibition (**Fig. 6D**). Tumour and plasma PK measurements 8- and 12-hours post dosing with alisertib indicated either micromolar or very high nanomolar tissue concentrations for this potent inhibitor (**Fig. 6E**). Alisertib is likely to have off-target activity against Aurora B at these high concentrations, which might be expected to decrease PH3, therefore overriding the increase in PH3 expected from Aurora A inhibiton[62,64].

CAM2602 induces growth suppression of tumour xenografts

Tolerability studies with 50, 100 and 150 mg/kg administered to NSG mice (daily dosing for 7 days, followed by 7 days without dosing) indicated that the highest dose examined of 150 mg/kg was tolerated without overt toxicity (**Fig. S8**). An efficacy study was performed using xenografted NSG mice bearing subcutaneous Jurkat cells implanted as solid tumours with a daily oral dose of either 100 or 150 mg/kg **CAM2602**, 20 mg/kg alisertib or vehicle for 26 days. Tumour volume measurements were taken three times per week during this time. The volume data indicated that vehicle-treated mice exhibited continuous tumour growth during the study, whereas the two doses of **CAM2602** were capable of successfully reducing tumour growth, the larger of the two doses having the greater effect (**Fig. 6G**). Alisertib had the greatest impact on tumour growth, likely due to the higher potency of this inhibitor. In agreement with earlier assessments of toxicity, there were no observations of toxic phenomena among the treated mice for the duration of the study and no evidence of loss of body weight (data not shown). Inhibition of Aurora kinases with ATP-competitive inhibitors has previously been linked to dose limiting toxicities such as bone marrow ablation and neutropenia[17,65]. Possible loss of blood cell lineages indicative of such toxicities were additionally analysed using blood samples taken from all mice upon completion of the efficacy study. These analyses indicated a very mild anaemic response in all non-vehicle animal dosing groups with a slight drop in haematocrit readings, but this was coincident in all cases with an elevation in reticulocyte count (**Fig. S9**).

Discussion

We have developed through fragment-based, structure-guided approaches a series of novel compounds that inhibit the PPI between Aurora A and TPX2. These are the first high-affinity ligands inhibiting this allosteric site and our lead compound **CAM2602** has pharmacological properties that enable it to be used in *in vivo* studies. These compounds occupy a hydrophobic pocket on the surface of Aurora A, discrete from its ATP-binding catalytic site, which forms the interaction surface for a linear N-terminal segment of the interacting peptide from TPX2. They displace critical interactions made by the Tyr8 and Tyr10 residues of TPX2 with Aurora A, directly inhibiting the binding of TPX2 to a key hotspot in Aurora A[34,66]. Notably, the compounds interact with Aurora residues that are not conserved in the closely related Aurora B kinase, providing a structural rationale for their high selectivity. Altogether, our work provides a blueprint for the development and optimization of a new class of Aurora A inhibitors that act by an allosteric mechanism.

Small molecule inhibition of Aurora A is an attractive strategy for the treatment of a wide range of human malignancies[3-8,15]. Consequently, several high-potency, orthosteric, ATP-competitive inhibitors of Aurora A have been developed[17]. Encouraging trial data have been seen for one such inhibitor, alisertib, across a range of cancers, but significant dose-limiting toxicities are consistently observed[31]. The promise of PPI inhibitors of kinases is that they bind to less conserved sites in the target and are more likely to exhibit better selectivity than orthosteric ATP-competitive molecules[38,67]. Therefore small molecule inhibitors targeting PPIs potentially exhibit fewer off-target toxicities and can have reduced propensity to develop resistance in cancer cells[38-40].

Here we report the identification of compounds interacting with Aurora A at the TPX2 binding site with the intention of inhibiting this important, activating PPI. These compounds were developed using a fragment-based structurally-enabled drug discovery strategy. The initial fragment hits were very weakly active but guided by structural biology we were able to increase target affinity by more than 4 orders of magnitude, clearly demonstrating the ability of fragment-based and structural biology approaches to develop potent PPI inhibitors when a suitable binding pocket is present. TPX2 is a particularly promising binding partner to block in this way, exhibiting a broad repertoire of

activity-promoting properties in relation to Aurora A[1,20,24]. Lead compounds were successfully identified that possess nano-molar binding affinities for the TPX2 binding site of Aurora A in FP and ITC assays and also demonstrate good ADMET properties. We find that these compounds are cytotoxic to cancer cells alone or in a synergistic combination with paclitaxel, with their cytotoxic effects proportional to target engagement marked by Aurora A mislocalisation and dephosphorylation on Thr288. We have demonstrated oral bioavailability and good pharmacokinetics for our lead compound **CAM2602**.

In a solid tumour xenograft model oral delivery of **CAM2602** successfully elicited biomarkers of target engagement, increasing PH3 positive cells and decreasing the proportion of those cells positive for P-Thr288 Aurora A, moreover this compound also reduced tumour growth. These results show that an inhibitor of the Aurora A-TPX2 PPI is a viable route to therapeutic intervention in cancer.

During the course of this work, Bayliss and co-workers have published the results of two crystallographic fragment screens against Aurora A.[34,35] Our target pocket, where tyrosines 8 and 10 of TPX2 bind, was identified as one of the hot spots for this PPI and a number of diverse fragments were found in this pocket, providing new possibilities for further development of Aurora A:TPX2 inhibitors.

The lack of overt toxicity seen *in vitro* and particularly in the *in vivo* studies with lead compound CAM2602 is noteworthy. Considering the high doses required to deliver our target tumour drug levels, it was possible that toxicity similar to that seen with ATP-competitive Aurora A inhibitors in the clinic[31] might impact the practical utility of **CAM2602** in the sustained multi-dose efficacy study. This apparent lack of toxicity may reflect the particularly high target-specificity which is characteristic of enzyme inhibition by the PPI mode rather than at the ATP-binding pocket.[38,39]

Using an earlier compound in our series, **5**, with an analogous structure and mode of action to **CAM2602** we were able to demonstrate drug synergy with Taxol in the pancreatic cell line PANC-1, emulating benefits previously observed for ATP-competitive Aurora A inhibitors. Considering the greatly limiting toxicities associated with Taxol in the clinic, a major therapeutic implication of these results could be the potential to greatly reduce required doses of Taxol when applied in combination with a drug targeting the Aurora A-TPX2 PPI. A prediction for Aurora A inhibition, including PPI-targeting agents, is the reversal of taxane resistance, which suggests a promising clinical opportunity to treat tumours with combinations of these agents[15,16,54,55]. Taxane resistance is a major clinical challenge with nearly half of all patients exhibiting primary resistance or eventually relapsing with treatment-resistant disease; agents that reverse taxane resistance would find utility in epithelial ovarian cancers, mammary adenocarcinomas and non-small cell lung carcinomas, for example[68-71]. In conclusion, we have developed a small molecule inhibitor of the Aurora A:TPX2 interaction, for which we provide a first example of efficacy in a xenograft model, providing a proof of concept for further development. In addition, the encouraging *in vitro* synergy demonstrated with Taxol suggests an important clinical modality for this new class of inhibitors.

Methods

Cell culture

HeLa, PANC-1 and Jurkat cells were maintained in humidified incubators at 37 °C, 5% CO_2 using either DMEM (HeLa and PANC-1: high glucose, GlutaMAX™ Supplement, pyruvate; ThermoFisher Scientific 10569010) or RPMI 1640 (Jurkat and PBMC: GlutaMAX™ Supplement, HEPES; ThermoFisher Scientific 72400021) media supplemented with 10% foetal bovine serum. As a positive

control in the high-content screening assays we made use of a previously reported stable HeLa FlpIn TREx cell line expressing a fusion mCherry-TPX2-1–43 protein which was inducible upon addition of doxycycline (0.5 mg ml^{-1})[37]. New vials of PBMC cells were obtained for each viability experiment (ATCC, PCS-800-011).

Viability assays

Cells were seeded onto sterile, flat-bottomed, 96-well tissue culture plates in antibiotic-free media; HeLa were seeded the day before treatment at a density of 5x10^3 per well, whereas Jurkat and PBMC cells were seeded at 2x10^4 or 1x10^5 per well, respectively, on the day of treatment. All wells per plate contained 100 μl of cells and/or media and the outermost wells of each plate contained media-only controls. On the day of treatment, 10-point, 2-fold dilution series of each compound were prepared in antibiotic-free media on separate, sterile, round bottomed 96-well plates. All series concentrations were adjusted to 5-fold higher than the intended final concentrations before 25 μl of these were then pipetted in triplicate to the flat-bottomed plates with cells, yielding a final volume of 125 μl per well. Matching DMSO-treatment dilution series were included in triplicate on each plate. Media-only edge wells received 25 μl of media to maintain equal final volumes across all wells on the plates, which were then sealed with sterile, breathable membranes beneath the plate lids and incubated in humidified incubators at 37 °C, 5% CO$_2$ for 72 hours. Depending on cell line, cell growth per well was assessed using the CellTiter-Blue assay (Jurkat cells, Promega) or sulforhodamine B assay (Hela). Cell-free control wells were used to calculate assay blanks for subtraction from assay values per treatment condition per plate; triplicate means of corresponding DMSO control well assay values for were used to determine fold-survival values for each compound treatment condition. GI$_{50}$ values were calculated from four-parameter dose-response curves that were fitted using Prism GraphPad software (La Jolla, CA).

High-content screening

The high-content imaging Aurora A mislocalisation and Thr288 dephosphorylation assays have been described previously by our lab[37]. Briefly, 24 hours after seeding 8x10^3 HeLa cells in 100 μl media per well of tissue-culture treated 96-well plates (ThermoFisher, 167008), the cells are treated with 9-point, 2-fold titrations of compound in media for 2 hours under standard tissue culture conditions. Drugging volumes were managed as described above for the viability assays (i.e. 25 μl is added to a final volume of 125 μl on cells to yield 5x dilution). Drugging media was supplemented to give a final concentration of 10 μM Velcade (Bortezomib, Selleck Chemicals) to reduce numbers of anaphase cells yielding false-positivity during image analysis. Following 2 hours incubation under drugging conditions, the plates were aspirated, fixed, permeabilised and stained as before[37].

Imaging of the plates was performed on an ImageXpress Micro Confocal High-Content Imaging System (Molecular Devices) using a 20x ELWD objective (optimal for 96-well plates with standard, 1.9 mm thick transparent bases) and laser autofocussing per field. For each well 12 non-overlapping fields in 3 fluorescent channels were acquired with bright-field optics and 2x2 binning, which allowed for approximately 100 mitotic cell observations per triplicate well. Custom Module Editor (CME) image analysis software (Molecular Devices) was used to quantify mitotic cell phenotypic responses, which were used to calculate assay endpoints.

Aurora A mislocalisation assay image data was analysed in CME by using Hoechst/DAPI channel image data to locate all individual nuclei per field. Corresponding TPX2/CY5 channel image data were used to identify the mitotic cell sub-populations in each field through TPX2-positivity of their nuclei. Intensity thresholds >100 times that of the image background were set in CME to distinguish DAPI and FITC channel signal from any noise. For each mitotic nucleus a top-hat filter with a 25 μm kernel

was used to define a fine mitotic spindle mask. Per mitotic spindle mask, the corresponding average Aurora A/FITC channel intensity was measured. The resulting cell-level data was exported and analysed in Excel whereby the highest spindle Aurora-A intensity in the darkest 10% of mitotic cells from untreated control wells was used to set a per-plate assay threshold below which Aurora-A was classified as delocalised from the spindle. The assay threshold was then applied across all mitotic cells recorded per well, the percentage of cells with Aurora-A intensity in the spindle mask below the threshold was reported as the percentage of mitotic cells per well with mislocalised Aurora A. The Thr288 dephosphorylation assay was performed and analysed the same way as for the mislocalisation assay, but substituted PH3 and P-Thr288 Aurora A antibodies for TPX2 and total Aurora A, respectively. In this case, PH3-positivity was used to identify mitotic cells and the mitotic spindle mask was replaced with a whole-nucleus mask for the purpose of measuring P-Thr288 loss. A percentage of mitotic cells per well exhibiting dephosphorylated Thr288 Aurora A measure used the same assay threshold calculation as used for the mislocalisation assay. Diagram of the imaging scheme and image analysis are shown in Supplemental **Fig. S11**.

Confocal microscopy

HeLa cells were grown on sterile type-I borosilicate glass cover slips placed in 6-well tissue culture plates with $2x10^5$ cells per well. 24 hours following seeding, the cells were treated as indicated, then the media was aspirated and the cells were fixed using ice-cold methanol for 10 minutes. Fixed cells were permeabilised with 0.1% Triton-X100, 0.1% TWEEN20 in PBS for 10 minutes at room temperature before being washed in blocking buffer (3% BSA, 0.1% TWEEN20 in PBS) for 30 minutes. Anti-Aurora A (Abcam, ab52973, 1:500) and anti-tubulin (Abcam, ab6160, 1:500) were diluted in blocking buffer and used to probe the cells for 30 minutes at room temperature. Excess antibody was washed with 3 rounds of 0.1% TWEEN20 in PBS, followed by probing with secondary antibodies (goat anti-rabbit Alexafluor 488, A11034, 1:500; goat anti-rat Alexafluor 647, A21247, 1:500, ThermoFisher Scientific) applied and washed as per the primary antibodies, supplemented with 4 µg/ml Hoeschst 33342. Imaging was performed on a Leica SP5 confocal microscope using a 100 × 1.4 NA oil objective. Maximum projection images were created with z-stacks taken at 1 µm intervals. Pixel intensities were kept sub-saturation. Laser exposure and detector settings were identical across an experiment to allow comparison between samples.

Flow cytometry

Jurkat cells from either tissue culture or resected tumour xenografts were washed, fixed and permeabilised using reagents from BD Biosciences (Stain Buffer, 554657; BD Cytofix, 554655; Perm Buffer III, 558050). Ideally, $1.5x10^6$ cells per sample were washed once with 500 µl cold Stain Buffer and transferred to clean 1.5ml centrifuge tubes. Samples were pelleted and aspirated before fixing with 250 µl BD Cytofix buffer following a brief vortex in the fixative and incubation on ice for 15 minutes. The fixed cells were then washed as before and subsequently pelleted and aspirated prior to being permeabilised by slow addition of 500 µl cold Perm Buffer III while vortexing. Samples were incubated on ice for 30 minutes then washed as before. The cells were then sequentially stained in three steps with anti-Aurora A P-Thr288 (1:100, Cell Signaling #3079), goat anti-rabbit Alexafluor555 (1:500, Life Technologies A21429) and finally AF647-conjugated anti-histone H3 (phospho-S10, 1:400, Cell Signaling #3458). For resected xenograft samples, AF488-conjugated human specific anti-CD3 (1:200, BD Pharmingen 557694) was included in the final staining step to allow exclusion of possible host cell contamination. The sequence of antibody staining is required to avoid species cross-reactivity between the chosen antibodies. The antibodies were applied to the cell samples in 100 µl of staining buffer, incubated for 30 minutes at room temperature with rotation and washed twice in 500 µl of stain buffer between each antibody step. Cells remained in the final wash supplemented with 4 µg/ml Hoechst 33342 and 250 µg/ml RNAse A. The cells were transferred to

flow cytometry tubes and incubated in the dark at room temperature for 30 minutes before being analysed. Analysis of flow cytometry samples was performed on a BD LSRFortessa equipped to excite the samples at 355nm, 488nm and 640nm and to resolve the fluorescent probes using separate detectors. Experiment data was analysed using FlowJo Ver.10 software (FlowJo, LLC). Gating strategies are shown in **Fig. S6**.

Western blotting

Total protein was isolated by directly lysing the cells in non-denaturing lysis buffer (50 mM HEPES-HCl pH7.4, 250 mM NaCl, 0.2% Triton X-100, 1 mM EDTA, 1 mM dithiothreitol, 1 mM NaF, 10 mM β-glycerophosphate, 0.1 mM Na_3VO_4, 1x Roche cOmplete protease inhibitors). Protein lysates (12 μg per lane) were resolved on SDS-PAGE gels, transferred onto an Immobilon-P, PVDF membrane (0.45 μm, Millipore), and probed with either anti-histone H3 (1:1000, NEB, 9715S) or anti-histone H3 (phosphor S10, 1:2000, Abcam, ab14955). Secondary HRP-conjugated antibodies were used (GE Healthcare) and the signal was detected using an Amersham enhanced chemiluminescence system (ECL, GE Healthcare).

In vivo studies

In vivo pharmacodynamics, tolerability and efficacy studies were carried out by Axis Bioservices Ltd (Northern Ireland). Pharmacokinetic work was done at WuXi AppTech (China). Female CD-1 mice were used in pharmacokinetics studies and female NOD-SCID gamma (NSG) mice were used for all other *in vivo* studies. For xenograft studies, Jurkat E6.1 cells (ATCC) were bulk-grown in RPMI 1640 media (GlutaMAX™ Supplement, HEPES; ThermoFisher Scientific 72400021) supplemented with 10% foetal bovine serum. Tumour cell implantation employed $2x10^7$ cells in matrigel per tumour, injected subcutaneously to the rear dorsum. Tumour volumes post-implantation were monitored using calliper measurements and mice were advanced for treatment when tumour volumes between 150mm-200mm^3 were reached. Where used, compounds were formulated in DMSO:20% HP-β-CD (2-hydroxypropyl-beta-cyclodextrin in PBS, 2.5:97.5) with pH adjusted to 7.6. All treatments were administered by oral gavage.

For pharmacodynamic biomarker studies, mice aged 5-7 weeks at time of implantation were administered single doses of the indicated treatments and were harvested for tumour resection and collection of whole blood by cardiac puncture at 0, 8 or 12 hours post-dosing. Plasma samples were submitted for PK analysis (Xenogesis Ltd.). Resected tumours were digested to single cell aspirates in dissociation buffer (RPMI medium supplemented with 5% FBS, Collagenase type I (200 U/ml) and DNase I (100 μg/ml)) for 30 minutes at 37°C with periodic vortexing and passed through a 70 μm filter with PBS washes. Tumour samples were cryogenically frozen and stored prior to being processed for flow cytometry as described above. Efficacy studies employed xenografted mice aged 6-8 weeks. Dosing was applied daily for 26 days and tumour volumes ($4/3πr^3$) were recorded three times per week by calliper measurements using three reference diameters to estimate geometric mean diameter. Samples were harvested 8 hours after the final dose. Tolerability studies used non-xenografted mice aged 6-8 weeks. Doses were applied daily for 7 days followed by a 7 day period with no treatment. Animal bodyweight, behaviour and appearance were monitored daily.

Synergy analysis

Drug synergy experiments using the Bliss independence model were performed as previously reported[55]. 96-well plates were seeded with $5x10^3$ PANC-1 cells per well 24 hours prior to drugging with a dilution series of each drug in an 8x8 checkerboard pattern of combinations. For both drugs, the lowest drug concentration value in each series was a no-drug vehicle control, which allowed for true single-agent dosing to be represented among the permutations of drug ratios tested. After SRB

staining to obtain the growth inhibition data, we used SynergyFinder webserver (https://synergyfinder.org/)[57]to identify synergistic drug combinations. The single-agent inhibition values were used to calculate a drug combination surface under the assumption of an additive effect. Regions of synergy were then detected by comparing observed combination data with the corresponding predicted values assuming additivity. In the final synergy plots, positive values indicate synergy regions, whereas negative difference values identify antagonistic effects.

Protein expression

Aurora A was expressed from pBAT4 or pHAT4 plasmid[72] in double cistronic construct with λ phosphatase, without which Aurora A was toxic to *E. coli*. Aurora A for biophysical assays was expressed from plasmid pBAT4-AurAS.003 which encoded for the kinase domain only (residues 126-390) of human Aurora A (Uniprot: O14965) followed by hexa-His tag. Deletion of the N-terminal localization domain implied the additional benefit of removing a region of the protein that was predicted to be intrinsically disordered. Further tailoring of the construct N- and C-termini was based on expression levels. For crystallography Aurora A contained also mutations Thr287Ala or Cys290Ala to reduce heterogeneity by activation loop phosphorylation and disulfide bond formation, respectively. For earlier compounds, a longer (residues 126-391) version of the protein without a C-terminal His-tag was used for crystallisation, as described in Janecek et al.[39] Aurora B protein was expressed from plasmid pNIC28-AurB (Addgene 39119).

Aurora A and Aurora B proteins were prepared with the same protocol. The protein expression was carried in BL21(DE3) strain (which was supplemented with pUBS520 plasmid for rare-Arg codon compensation for Aurora A) in 2YT media with 100 μg/ml of ampicillin. The cells were grown in shaker flasks to OD of 0.8-1.0 and expression induced with 400 μM isopropyl-thio-β-glycopyranoside for 3 hours at 37 °C. Cells were harvested by centrifugation and pellets stored at -20 °C. Cells were resuspended in 50 mM HEPES pH 7.4, 1 M NaCl, 100 mM Mg Acetate, 1mM ATP/1mM ADP, 25 mM Imidazole, 5 mM β-mercaptoethanol, with one tablet of protease inhibitors (cOmplete Protease Inhibitor Cocktails, Roche) and 500 μl of 2mg/ml DNaseI (Sigma: DN25). Cells were lysed with sonication or using an Emulsiflex homogeniser and lysate clarified by centrifugation at 30,000 *g* for 30 mins at 4 °C. The supernatant was filtered and protein purified with automated two-step protocol using an ÄKTA Pure chromatography system. The protein was captured in 5 ml FF HisTrap column (Cytiva) and washed with 50 mM HEPES/Na pH 7.4, 500 mM NaCl, 100 mM magnesium acetate, 1 mM ATP/1 mM ADP, 40 mM Imidazole, 5mM β-mercaptoethanol, 10% v/v glycerol until baseline stabilised. Protein was eluted in reverse flow with 50 mM HEPES/Na pH 7.4, 500 mM NaCl, 100 mM Mg Acetate, 1 mM ATP/ 1 mM ADP, 600 mM Imidazole, 5 mM β-mercaptoethanol, 10% v/v glycerol and the eluted protein directed to injection loop and injected directly to HiLoad 16/60 Superdex 75 pg column (Cytiva) which had been equilibrated with 50 mM HEPES pH 7.4, 50 mM NaCl, 100 mM Mg Acetate, 1 mM ADP, 0.5 mM TCEP, 10% v/v glycerol and column ran at 1 ml/min. Peak fraction was pooled, concentrated and stored in flash-frozen aliquots at -80 °C.

TPX2 peptide (residues 7-43, Uniprot: Q9ULW0) with C-terminal GGGCSS tail was expressed in *E. coli* as a GB1 fusion with an N-terminal His-tag and HRV 3C protease cleavage site for tag removal in vector pOP3BP, as described above. A pellet from 2 litre culture was resuspended in 50 mM HEPES pH 7.4, 500 mM NaCl, 40 mM imidazole, 10% glycerol, 0.5 mM TCEP and 500 μl of DNaseI (2 mg/ml) and lysed using a sonicator. Lysate was centrifuged for 30 min at 15,0000 *g* and filtered supernatant loaded on 1 ml gravity flow Ni Sepharose column (Cube Biotech). After washing with lysis buffer, the protein was eluted with 50 mM HEPES pH 7.4, 500 mM NaCl, 300 mM imidazole, 10% glycerol, 0.5 mM TCEP. Peak fractions were pooled and buffer exchanged with PD-10 column to remove imidazole and glycerol. Alexa Fluor™ 488 C5 Maleimide (catalogue no. A10254, Thermo Fisher

Scientific) was added to the protein sample in 25-fold molar excess to label the C-terminal cysteine for 2 h at room temperature. Reaction was terminated with excess cysteine and protein cleaved with HRV 3C protease overnight. The cleaved protein was passed through second Ni Sepharose column to remove fusion protein and uncleaved material. Labelled peptide was purified by reversed phase chromatography using HiChrom 300 Å 4.6x250 mm C18 column with gradient elution from 10 % acetonitrile, 0.1 % trifluoroacetic acid to 90 % acetonitrile at 3ml/min flow rate, dried under vacuum, resuspended in 50 mM HEPES pH 7.4, 100 mM Mg acetate, 50 mM NaCl and stored at -80 °C in dark.

Fluorescence polarisation (FP) assay

The FP assay was done using a BMG Pherastar FS plate reader with a gain of 20% and target 90 mP. The Kd for TPX2 binding to Aurora A was determined to be 1.2 nM by direct titration of up to 200 nM of Aurora A protein to 11 nM labelled TPX2 peptide in 100 mM HEPES pH 7.4, 100 mM magnesium acetate, 50 mM NaCl, 0.02% P20, 1 mM DTT, 1 mM ATP, 10% (v/v) DMSO. The competition FP assay was run in the same buffer with 10 nM TPX2 peptide and 30 nM Aurora A. 12 concentrations of compounds from 1 µM to 2 mM were used as competitors in triplicate. The data was monitored for both anisotropy and for change in total fluorescence to account for any artefacts, such as compound interference or aggregation. The resulting competitive binding isotherms were measured and fitted using the expression described by Wang[73] using Pro Fit software package (Quan Soft).

Isothermal titration calorimetry

Isothermal titration calorimetry (ITC) was performed using a Microcal itc200 instrument at 25 °C, in the following experimental buffer (unless specifically indicated otherwise): 0.1 M HEPES/Na pH 7.4, 0.1 M magnesium acetate, 0.05 M NaCl, with the addition of 10% v/v DMSO, fresh 1 mM ATP and fresh 0.25 mM TCEP.

Prior the experiment, Aurora A protein was thawed and buffer exchanged in the experimental buffer using NAP-5 Columns (GE Healthcare). Experiments typically involved titrating 25 µM of protein in the sample cell with 300 µM of compound in the syringe. The raw ITC data were fitted using a single site binding model using the Microcal ITC LLC data analysis program in the Origin 7.0 package.

Crystallisation and structure determination

To solution of 3.8 mg/ml of Aurora A SilverBullet screen solution 82 (Hampton Research) trans-1,2-cyclohexanedicarboxylic acid was added to final concentration of 8% by volume and the sample was centrifuged for 5 minutes at room temperature at maximum speed in a microcentrifuge. Crystallisation was done in 96-well "MRC" plates (Molecular Dimensions) using a Mosquito nanoliter robot (TTP Labtech) with 300 nl + 300 nl drop with 30% PEG5000 MME (28-32%), 0.1M $(NH_4)_2SO_4$, 0.1 M MES pH 6.5 as the mother liquor. For soaking 1 µl of 100 mM compound in DMSO was diluted with 9 µl of 30% PEG5000 MME (28-32%), 0.1M $(NH_4)_2SO_4$, 0.1 M MES pH 6.5 and added to the crystals for between 2 h and overnight. Crystals were collected into a nylon loop and flash cooled to in liquid nitrogen and stored for data collection. Data collection was typically done for 180 images at 1° oscillation per image. Data reduction and automatic structure determination was done using the pipedream work-flow from Global Phasing Ltd with automatic ligand fitting. Ligand restraints were generated with grade and mogul from CCDC. Structure was analysed and corrected using Coot and refined with Buster TNT. Final ligand electron densities are shown in **Fig. S10**. The structure factors and coordinates have been deposited to Protein Data Bank under access codes: 8C1M, 8C15, 8C1D, 8C1M, 8C15, 8C1D, 8C1H, 8C14, 8C1I, 8C1K with data collection and structrure refinement statistics listed in **table S4**.

Abbreviations

SAR, Structure Activity Relationship;

Acknowledgements

Funding

Author Contributions

JS, CA, DS, MH, TLB and ARV – envisaged the project, wrote the grant application and supervised the work. JS and DES led the project for part of the time. DES, TPCR, JF, RS, CD, EA, and JS contributed to compound design and/or chemical synthesis. AH was in charge of modelling and data management and contributed to compound design. GF, MR and MR were in charge of crystallography and 3D structure interpretation. TM, MR, BB and XW were responsible for protein biochemistry and biophysical analyses. SRS, EGA, AA-L and GM were responsible for cell biology and animal experiments. TP advised on medicinal chemistry. SRS, DES, JS, MH and ARV wrote the paper. All authors have edited the manuscript and contributed to their part of the data analyses.

References

1   Asteriti, I. A., Rensen, W. M., Lindon, C., Lavia, P. & Guarguaglini, G. The Aurora-A/TPX2 complex: a novel oncogenic holoenzyme? *Biochim Biophys Acta* **1806**, 230-239, doi:10.1016/j.bbcan.2010.08.001 (2010).
2   Fu, J., Bian, M., Jiang, Q. & Zhang, C. Roles of Aurora kinases in mitosis and tumorigenesis. *Mol Cancer Res* **5**, 1-10, doi:10.1158/1541-7786.Mcr-06-0208 (2007).
3   Lassus, H., Staff, S., Leminen, A., Isola, J. & Butzow, R. Aurora-A overexpression and aneuploidy predict poor outcome in serous ovarian carcinoma. *Gynecol Oncol* **120**, 11-17, doi:10.1016/j.ygyno.2010.09.003 (2011).
4   Lee, E. C., Frolov, A., Li, R., Ayala, G. & Greenberg, N. M. Targeting Aurora kinases for the treatment of prostate cancer. *Cancer Res* **66**, 4996-5002, doi:10.1158/0008-5472.Can-05-2796 (2006).
5   Li, D. *et al.* Overexpression of oncogenic STK15/BTAK/Aurora A kinase in human pancreatic cancer. *Clin Cancer Res* **9**, 991-997 (2003).
6   Goldberg, S. L. *et al.* An exploratory phase 2 study of investigational Aurora A kinase inhibitor alisertib (MLN8237) in acute myelogenous leukemia and myelodysplastic syndromes. *Leuk Res Rep* **3**, 58-61, doi:10.1016/j.lrr.2014.06.003 (2014).
7   Ochi, T., Fujiwara, H. & Yasukawa, M. Aurora-A kinase: a novel target both for cellular immunotherapy and molecular target therapy against human leukemia. *Expert Opin Ther Targets* **13**, 1399-1410, doi:10.1517/14728220903307483 (2009).
8   Shafer, D. & Grant, S. Update on rational targeted therapy in AML. *Blood Rev* **30**, 275-283, doi:10.1016/j.blre.2016.02.001 (2016).
9   Zhou, H. *et al.* Tumour amplified kinase STK15/BTAK induces centrosome amplification, aneuploidy and transformation. *Nat Genet* **20**, 189-193, doi:10.1038/2496 (1998).

10   D'Assoro, A. B., Haddad, T. & Galanis, E. Aurora-A Kinase as a Promising Therapeutic Target in Cancer. *Front Oncol* **5**, 295, doi:10.3389/fonc.2015.00295 (2015).

11   van Gijn, S. E. *et al.* TPX2/Aurora kinase A signaling as a potential therapeutic target in genomically unstable cancer cells. *Oncogene* **38**, 852-867, doi:10.1038/s41388-018-0470-2 (2019).

12   Do, T. V., Hirst, J., Hyter, S., Roby, K. F. & Godwin, A. K. Aurora A kinase regulates non-homologous end-joining and poly(ADP-ribose) polymerase function in ovarian carcinoma cells. *Oncotarget* **8**, 50376-50392, doi:10.18632/oncotarget.18970 (2017).

13   Kivinummi, K. *et al.* The expression of AURKA is androgen regulated in castration-resistant prostate cancer. *Sci Rep* **7**, 17978, doi:10.1038/s41598-017-18210-3 (2017).

14   Shah, K. N. *et al.* Aurora kinase A drives the evolution of resistance to third-generation EGFR inhibitors in lung cancer. *Nat Med* **25**, 111-118, doi:10.1038/s41591-018-0264-7 (2019).

15   Cirak, Y., Furuncuoglu, Y., Yapicier, O., Aksu, A. & Cubukcu, E. Aurora A overexpression in breast cancer patients induces taxane resistance and results in worse prognosis. *J BUON* **20**, 1414-1419 (2015).

16   Anand, S., Penrhyn-Lowe, S. & Venkitaraman, A. R. AURORA-A amplification overrides the mitotic spindle assembly checkpoint, inducing resistance to Taxol. *Cancer Cell* **3**, 51-62 (2003).

17   Bavetsias, V. & Linardopoulos, S. Aurora Kinase Inhibitors: Current Status and Outlook. *Front Oncol* **5**, 278, doi:10.3389/fonc.2015.00278 (2015).

18   de Groot, C. O. *et al.* A Cell Biologist's Field Guide to Aurora Kinase Inhibitors. *Front Oncol* **5**, 285, doi:10.3389/fonc.2015.00285 (2015).

19   Damodaran, A. P., Vaufrey, L., Gavard, O. & Prigent, C. Aurora A Kinase Is a Priority Pharmaceutical Target for the Treatment of Cancers. *Trends Pharmacol Sci* **38**, 687-700, doi:10.1016/j.tips.2017.05.003 (2017).

20   Bird, A. W. & Hyman, A. A. Building a spindle of the correct length in human cells requires the interaction between TPX2 and Aurora A. *J Cell Biol* **182**, 289-300, doi:10.1083/jcb.200802005 (2008).

21   Kufer, T. A. *et al.* Human TPX2 is required for targeting Aurora-A kinase to the spindle. *J Cell Biol* **158**, 617-623, doi:10.1083/jcb.200204155 (2002).

22   Garrido, G. & Vernos, I. Non-centrosomal TPX2-Dependent Regulation of the Aurora A Kinase: Functional Implications for Healthy and Pathological Cell Division. *Front Oncol* **6**, 88, doi:10.3389/fonc.2016.00088 (2016).

23   Giubettini, M. *et al.* Control of Aurora-A stability through interaction with TPX2. *J Cell Sci* **124**, 113-122, doi:10.1242/jcs.075457 (2011).

24   Bayliss, R., Sardon, T., Vernos, I. & Conti, E. Structural basis of Aurora-A activation by TPX2 at the mitotic spindle. *Mol Cell* **12**, 851-862 (2003).

25   Tsai, M. Y. *et al.* A Ran signalling pathway mediated by the mitotic kinase Aurora A in spindle assembly. *Nat Cell Biol* **5**, 242-248, doi:10.1038/ncb936 (2003).

26   Perez de Castro, I. & Malumbres, M. Mitotic Stress and Chromosomal Instability in Cancer: The Case for TPX2. *Genes Cancer* **3**, 721-730, doi:10.1177/1947601912473306 (2012).

27   Goldenson, B. & Crispino, J. D. The aurora kinases in cell cycle and leukemia. *Oncogene* **34**, 537-545, doi:10.1038/onc.2014.14 (2015).

28   Otto, T. & Sicinski, P. Cell cycle proteins as promising targets in cancer therapy. *Nat Rev Cancer* **17**, 93-115, doi:10.1038/nrc.2016.138 (2017).

29   Sarvagalla, S. & Coumar, M. S. Structural Biology Insight for the Design of Sub-type Selective Aurora Kinase Inhibitors. *Curr Cancer Drug Targets* **15**, 375-393 (2015).

30   Carmena, M. & Earnshaw, W. C. The cellular geography of aurora kinases. *Nat Rev Mol Cell Biol* **4**, 842-854, doi:10.1038/nrm1245 (2003).

31   Tayyar, Y., Jubair, L., Fallaha, S. & McMillan, N. A. J. Critical risk-benefit assessment of the novel anti-cancer aurora a kinase inhibitor alisertib (MLN8237): A comprehensive review of

the clinical data. *Crit Rev Oncol Hematol* **119**, 59-65, doi:10.1016/j.critrevonc.2017.09.006 (2017).

32 Manfredi, M. G. *et al.* Characterization of Alisertib (MLN8237), an investigational small-molecule inhibitor of aurora A kinase using novel in vivo pharmacodynamic assays. *Clin Cancer Res* **17**, 7614-7624, doi:10.1158/1078-0432.Ccr-11-1536 (2011).

33 Asteriti, I. A. *et al.* Identification of small molecule inhibitors of the Aurora-A/TPX2 complex. *Oncotarget* **8**, 32117-32133, doi:10.18632/oncotarget.16738 (2017).

34 McIntyre, P. J. *et al.* Characterization of Three Druggable Hot-Spots in the Aurora-A/TPX2 Interaction Using Biochemical, Biophysical, and Fragment-Based Approaches. *ACS Chem Biol*, doi:10.1021/acschembio.7b00537 (2017).

35 Zhang, R. *et al.* Construction of a Shape-Diverse Fragment Set: Design, Synthesis and Screen against Aurora-A Kinase. *Chemistry* **25**, 6831-6839, doi:10.1002/chem.201900815 (2019).

36 Gustafson, W. C. *et al.* Drugging MYCN through an allosteric transition in Aurora kinase A. *Cancer Cell* **26**, 414-427, doi:10.1016/j.ccr.2014.07.015 (2014).

37 Janecek, M. *et al.* Allosteric modulation of AURKA kinase activity by a small-molecule inhibitor of its protein-protein interaction with TPX2. *Sci Rep* **6**, 28528, doi:10.1038/srep28528 (2016).

38 Fang, Z., Grutter, C. & Rauh, D. Strategies for the selective regulation of kinases with allosteric modulators: exploiting exclusive structural features. *ACS Chem Biol* **8**, 58-70, doi:10.1021/cb300663j (2013).

39 Wu, P., Clausen, M. H. & Nielsen, T. E. Allosteric small-molecule kinase inhibitors. *Pharmacol Ther* **156**, 59-68, doi:10.1016/j.pharmthera.2015.10.002 (2015).

40 Narvaez, A. J. *et al.* Modulating Protein-Protein Interactions of the Mitotic Polo-like Kinases to Target Mutant KRAS. *Cell Chem Biol*, doi:10.1016/j.chembiol.2017.07.009 (2017).

41 Zhang, J. *et al.* Targeting Bcr-Abl by combining allosteric with ATP-binding-site inhibitors. *Nature* **463**, 501-506, doi:10.1038/nature08675 (2010).

42 Lee, J. K. *et al.* N-Myc Drives Neuroendocrine Prostate Cancer Initiated from Human Prostate Epithelial Cells. *Cancer Cell* **29**, 536-547, doi:10.1016/j.ccell.2016.03.001 (2016).

43 Groom, C. R., Bruno, I. J., Lightfoot, M. P. & Ward, S. C. The Cambridge Structural Database. *Acta Crystallogr B Struct Sci Cryst Eng Mater* **72**, 171-179, doi:10.1107/S2052520616003954 (2016).

44 Bayliss, R. *et al.* Determinants for Aurora-A activation and Aurora-B discrimination by TPX2. *Cell Cycle* **3**, 404-407 (2004).

45 Keen, N. & Taylor, S. Aurora-kinase inhibitors as anticancer agents. *Nat Rev Cancer* **4**, 927-936, doi:10.1038/nrc1502 (2004).

46 Gong, X. *et al.* Aurora A Kinase Inhibition Is Synthetic Lethal with Loss of the RB1 Tumor Suppressor Gene. *Cancer Discov* **9**, 248-263, doi:10.1158/2159-8290.Cd-18-0469 (2019).

47 Kaestner, P., Stolz, A. & Bastians, H. Determinants for the efficiency of anticancer drugs targeting either Aurora-A or Aurora-B kinases in human colon carcinoma cells. *Mol Cancer Ther* **8**, 2046-2056, doi:10.1158/1535-7163.Mct-09-0323 (2009).

48 Lee, C. C., Lin, S. J., Cheng, P. J. & Kuo, M. L. The regulatory function of umbilical cord blood CD4(+) CD25(+) T cells stimulated with anti-CD3/anti-CD28 and exogenous interleukin (IL)-2 or IL-15. *Pediatr Allergy Immunol* **20**, 624-632, doi:10.1111/j.1399-3038.2008.00843.x (2009).

49 Stallwood, Y. *et al.* Small interfering RNA-mediated knockdown of notch ligands in primary CD4+ T cells and dendritic cells enhances cytokine production. *J Immunol* **177**, 885-895 (2006).

50 Girdler, F. *et al.* Validating Aurora B as an anti-cancer drug target. *J Cell Sci* **119**, 3664-3675, doi:10.1242/jcs.03145 (2006).

51 Marumoto, T. *et al.* Aurora-A kinase maintains the fidelity of early and late mitotic events in HeLa cells. *J Biol Chem* **278**, 51786-51795, doi:10.1074/jbc.M306275200 (2003).

52   Chakravarty, A. *et al.* Phase I assessment of new mechanism-based pharmacodynamic biomarkers for MLN8054, a small-molecule inhibitor of Aurora A kinase. *Cancer Res* **71**, 675-685, doi:10.1158/0008-5472.Can-10-1030 (2011).

53   Macarulla, T. *et al.* Phase I study of the selective Aurora A kinase inhibitor MLN8054 in patients with advanced solid tumors: safety, pharmacokinetics, and pharmacodynamics. *Mol Cancer Ther* **9**, 2844-2852, doi:10.1158/1535-7163.Mct-10-0299 (2010).

54   Giovinazzi, S., Morozov, V. M., Summers, M. K., Reinhold, W. C. & Ishov, A. M. USP7 and Daxx regulate mitosis progression and taxane sensitivity by affecting stability of Aurora-A kinase. *Cell Death Differ* **20**, 721-731, doi:10.1038/cdd.2012.169 (2013).

55   Lin, Y. *et al.* Paclitaxel and CYC3, an aurora kinase A inhibitor, synergise in pancreatic cancer cells but not bone marrow precursor cells. *Br J Cancer* **107**, 1692-1701, doi:10.1038/bjc.2012.450 (2012).

56   Di Veroli, G. Y. *et al.* Combenefit: an interactive platform for the analysis and visualization of drug combinations. *Bioinformatics* **32**, 2866-2868, doi:10.1093/bioinformatics/btw230 (2016).

57   Zheng, S. *et al.* SynergyFinder Plus: Toward Better Interpretation and Annotation of Drug Combination Screening Datasets. *Genomics Proteomics Bioinformatics* **20**, 587-596, doi:10.1016/j.gpb.2022.01.004 (2022).

58   Carol, H. *et al.* Efficacy and pharmacokinetic/pharmacodynamic evaluation of the Aurora kinase A inhibitor MLN8237 against preclinical models of pediatric cancer. *Cancer Chemother Pharmacol* **68**, 1291-1304, doi:10.1007/s00280-011-1618-8 (2011).

59   Dees, E. C. *et al.* Phase I study of aurora A kinase inhibitor MLN8237 in advanced solid tumors: safety, pharmacokinetics, pharmacodynamics, and bioavailability of two oral formulations. *Clin Cancer Res* **18**, 4775-4784, doi:10.1158/1078-0432.Ccr-12-0589 (2012).

60   Cervantes, A. *et al.* Phase I pharmacokinetic/pharmacodynamic study of MLN8237, an investigational, oral, selective aurora a kinase inhibitor, in patients with advanced solid tumors. *Clin Cancer Res* **18**, 4764-4774, doi:10.1158/1078-0432.Ccr-12-0571 (2012).

61   Giet, R. & Glover, D. M. Drosophila aurora B kinase is required for histone H3 phosphorylation and condensin recruitment during chromosome condensation and to organize the central spindle during cytokinesis. *J Cell Biol* **152**, 669-682 (2001).

62   Nair, J. S. & Schwartz, G. K. MLN-8237: A dual inhibitor of aurora A and B in soft tissue sarcomas. *Oncotarget* **7**, 12893-12903, doi:10.18632/oncotarget.7335 (2016).

63   Neel, N. F. *et al.* Response to MLN8237 in pancreatic cancer is not dependent on RalA phosphorylation. *Mol Cancer Ther* **13**, 122-133, doi:10.1158/1535-7163.Mct-12-1232 (2014).

64   Palani, S. *et al.* Preclinical pharmacokinetic/pharmacodynamic/efficacy relationships for alisertib, an investigational small-molecule inhibitor of Aurora A kinase. *Cancer Chemother Pharmacol* **72**, 1255-1264, doi:10.1007/s00280-013-2305-8 (2013).

65   Keen, N. & Taylor, S. Mitotic drivers--inhibitors of the Aurora B Kinase. *Cancer Metastasis Rev* **28**, 185-195, doi:10.1007/s10555-009-9184-9 (2009).

66   Rossmann, M., S, J. G., Moschetti, T., Dinan, M. & Hyvonen, M. Development of a multipurpose scaffold for the display of peptide loops. *Protein Eng Des Sel* **30**, 419-430, doi:10.1093/protein/gzx017 (2017).

67   Lu, S., Li, S. & Zhang, J. Harnessing allostery: a novel approach to drug discovery. *Med Res Rev* **34**, 1242-1285, doi:10.1002/med.21317 (2014).

68   Ehrlichova, M. *et al.* The association of taxane resistance genes with the clinical course of ovarian carcinoma. *Genomics* **102**, 96-101, doi:10.1016/j.ygeno.2013.03.005 (2013).

69   Murray, S., Briasoulis, E., Linardou, H., Bafaloukos, D. & Papadimitriou, C. Taxane resistance in breast cancer: mechanisms, predictive biomarkers and circumvention strategies. *Cancer Treat Rev* **38**, 890-903, doi:10.1016/j.ctrv.2012.02.011 (2012).

70   Visconti, R. & Grieco, D. Fighting tubulin-targeting anticancer drug toxicity and resistance. *Endocr Relat Cancer* **24**, T107-T117, doi:10.1530/erc-17-0120 (2017).

71   Wang, S., Qiu, J., Shi, Z., Wang, Y. & Chen, M. Nanoscale drug delivery for taxanes based on the mechanism of multidrug resistance of cancer. *Biotechnol Adv* **33**, 224-241, doi:10.1016/j.biotechadv.2014.10.011 (2015).

72   Peränen, J., Rikkonen, M., Hyvönen, M. & Kääriäinen, L. T7 vectors with modified T7lac promoter for expression of proteins in Escherichia coli. *Anal Biochem* **236**, 371-373, doi:10.1006/abio.1996.0187 (1996).

73   Wang, Z. X. An exact mathematical expression for describing competitive binding of two different ligands to a protein molecule. *FEBS Lett* **360**, 111-114, doi:10.1016/0014-5793(95)00062-e (1995).